Published in "Physical Review B 97 (19): 195110, 2018"
which should be cited to refer to this work.

Brownian dynamics of colloidal microspheres with tunable elastic properties from soft to hard

Jiwon Yoon[a,d], Frédéric Cardinaux[a], Clayton Lapointe[a], Chi Zhang[a], Thomas G. Mason[b,c], Kyung Hyun Ahn[d], Frank Scheffold[a,*]

[a] Department of Physics, University of Fribourg, Chemin du Musée 3, 1700 Fribourg, Switzerland
[b] Department of Chemistry and Biochemistry, University of California, Los Angeles, CA 90095, USA
[c] Department of Physics and Astronomy, University of California, Los Angeles, CA 90095, USA
[d] School of Chemical Engineering, Seoul National University, 599 Kwanak-ro Kwanak-gu, South Korea

GRAPHICAL ABSTRACT

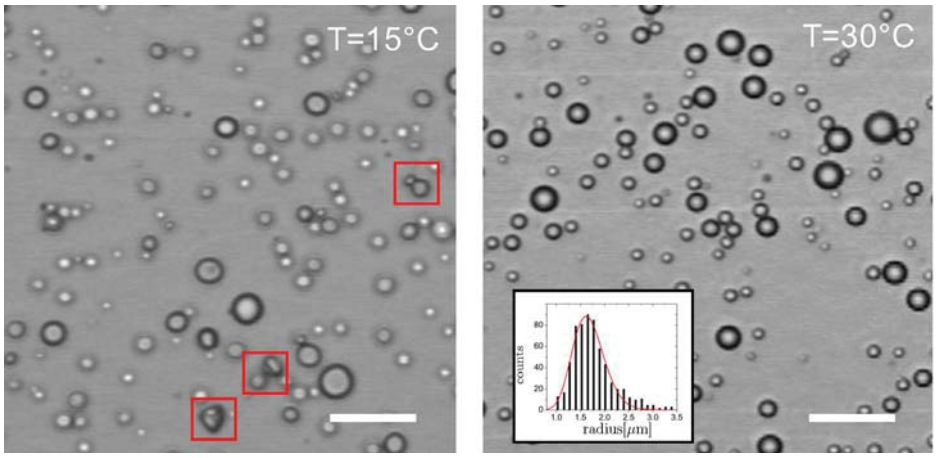

ARTICLE INFO

Keywords:
Emulsions
Colloids
Shape fluctuations
Wax

ABSTRACT

We study the Brownian thermal motion of a colloidal model system made by emulsifying hot liquid α-eicosene wax into an aqueous surfactant solution of sodium dodecyl sulfate (SDS). When this waxy oil-in-water emulsion is cooled below α-eicosene's melting point of $T_c \simeq 25\,^{\circ}\mathrm{C}$, the microscale emulsion droplets solidify, effectively yielding a dispersed particulate system. So, the interiors of these wax droplets can be tuned from a viscous liquid to an elastic solid through very modest changes in absolute temperature. Using the multiple light scattering technique of diffusing wave spectroscopy (DWS), which is very sensitive to small-scale motion and shape fluctuations of dispersed colloidal objects, we show that the thermal fluctuations of the interfaces of these liquid droplets at higher temperature, seen in the DWS intensity–intensity correlation function at early times, effectively disappear when these droplets solidify at lower temperature. Thus, we show that the early-time behavior of this DWS correlation function can be used to probe mechanical properties of viscoelastic soft materials dispersed as droplets.

* Corresponding author.
E-mail address: Frank.Scheffold@unifr.ch (F. Scheffold).

1. Introduction

Soft colloidal particles are ubiquitous in daily life and have been widely used in industry for centuries. They can be found, for example, as constituents of mayonnaise, lotions, thickeners or drilling fluids. The remarkable features of soft particle systems, such as emulsions and microgels, can be related directly to their interfacial deformability. Since soft particles dissipate stress by compression or by deforming their interface upon shear, systems can be prepared at higher volume fractions ϕ than imposed by the random close packing limit of hard spheres $\phi_{rcp} \simeq 0.64$ [1–6]. In experiments, one can distinguish three typical cases. On the *soft* side one can find highly deformable particles with a fuzzy interface such as microgels or weakly screened charged particles with long range repulsive interactions [4,7–9]. On the *stiff side*, and in the limit of negligible compression or deformability, the case of hard spheres is approached. In an experiment the hard sphere limit can be realized, to within a good approximation, by preparing sterically stabilized solid particles such as PMMA spheres used in many studies [10–12]. A plethora of theoretical and fundamental experimental work has been dedicated to this idealized case [8]. Moreover, many dispersion properties can be mapped on this simplified case by introducing an effective volume fraction taking account for finite ranged repulsive interactions [13]. Dispersions made from repulsive particles have been studied widely and under a variety of different conditions and in mixtures [14]. What has been lacking until now are studies on a particle model system with a sharp interface where the properties of the particles could be tuned in situ from deformable to hard without leading to aggregation. The sharp interface is of key importance for a clear definition of the volume fraction and the random close packing or jamming condition [15]. Equally, in computer simulations of soft spheres the interactions are usually modeled by an harmonic or anharmonic repulsive interaction potential with a sharp onset upon contact [16,17]. Tunable model systems such as microgels, however, generally feature rather fuzzy interfaces which makes it difficult to pinpoint the condition for marginal particle–particle contacts – also known as the isostatic condition – where a percolated network of contacts can bear a finite load. The latter is a hallmark of the athermal jamming condition [16–19]. Emulsion droplets are probably the closest model system for such deformable, but elastic colloidal objects that possess a sharp, nanoscale liquid-liquid interface [2,17].

In this study, we set out to design and study the Brownian thermal motion of a tunable model systems based on emulsified wax with properties that can be tuned from liquid to solid. We emulsify α-eicosene and use depletion fractionation to obtain a fairly uniform oil-in-water emulsion. α-eicosene has a critical temperature (melting point) of $T_c \simeq 25$ °C. Cooling below this transition point, the emulsion droplets solidify. The transition allows us to control the single particle elastic properties, which affects thermal fluctuations of the droplet interface. These changes are not associated with any significant change of volume fraction or particle size and can be tuned by temperature. In the present study we analyze the dynamic and optical properties of dense α-eicosene suspensions at two selected temperatures, $T = 15$ °C and $T = 30$ °C. These temperatures are chosen far away from T_c, respectively, and therefore we expect the droplets to be uniformly liquid above T_c and solid below T_c. We discuss the effect of changes of the particle deformability, from soft to hard, on the properties of such emulsions. To access the microscopic dynamic sample properties we use diffusing wave spectroscopy (DWS) [20,21], a dynamic light scattering method ideally suited to study thermal motion on small length scales in a highly multiple scattering and dense sample. In an emulsion system, liquid droplets have deformable interfaces which are subject to thermal fluctuations. At short time scale, shape fluctuations have a magnitude similar to the center of mass diffusion and the fluid hydrodynamics around the droplet, hence, these contributions can be quantified using DWS [22]. However, when the droplets turn solid these fluctuations are frozen.

2. Experimental

2.1. Materials

We study α-eicosene-in-water emulsions stabilized by 10 mM sodium dodecylsulfate (SDS > 90%, from Sigma–Aldrich) based on a procedure initially reported in [23]. We chose α-eicosene wax (1-eicosene, $H_2C{=}CH(CH_2)_{17}CH_3$, Sigma–Aldrich, technical grade, purity > 80%) as the dispersed phase because in the bulk it solidifies at temperatures below T_c. The melting point specified by the manufacturer is $T_c \sim 25$–30 °C. We determine the density of α-eicosene in house to $\rho_{wax} \simeq 0.8\,g/cm^3$, in agreement with literature specifications for the pure substance $\rho_{wax} = 0.79 g/cm^3$[24]. Within the limited resolution of our volumetric measurements, we do not observe a significant temperature dependence of ρ_{wax} over the range 50–10 °C studied. The value for the refractive index $n = 1.44$ is taken from the literature [24]. To access the viscosity in the liquid phase and the melting point of our batch we have performed temperature sweeps from 50 °C to 10 °C while measuring the zero shear viscosity η_{wax} with a commercial rheometer (MCR 502, Anton Paar, Austria). We find $\eta_{wax} = 4$ cP for $T = 30$ °C compared to the viscosity of water $\eta = 0.8$ cP at the same temperature. The viscosity η_{wax} sharply increases below $T_c = 25.4$ °C indicating the liquid solid transition is located around $T_c \simeq 25$ °C. Oil droplets are then prepared at $T \geq 50$ °C by shear rupturing of a crude emulsion in a custom made Couette cell [25] and subsequent size fractionation using depletion induced creaming [23,26]. We note that uniform discotic wax particles can also be produced via electrospray emulsification [27]. In our case, however, the resulting suspension is composed of spherical droplets having an average diameter $2\overline{R} = 3.36\,\mu m$ and a size polydispersity in the number distribution of $\Delta R/\overline{R} \simeq 0.195$, Fig. 1. The size distribution is derived from brightfield microscopy via particle imaging analysis, as shown in the inset of Fig. 1. We monitor the emulsions repeatedly over time by microscopy and find them to be stable for

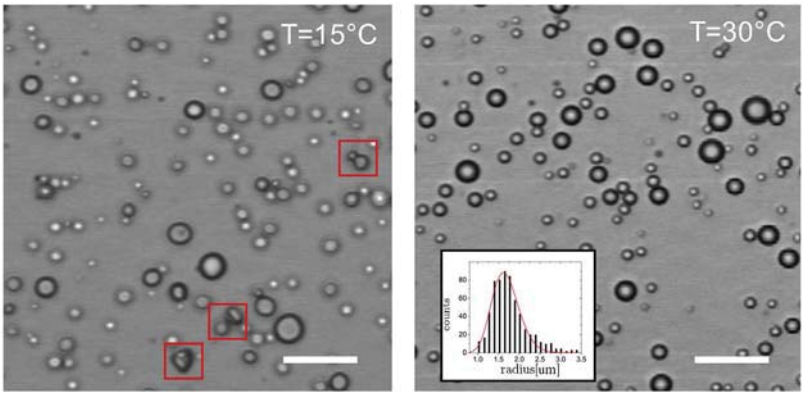

Fig. 1. Bright field microscopy image of the α-eicosene-in-water emulsions droplets, scale bar 20 μm. Left: Solidified droplets at $T \sim 15$ °C. Some of the droplets acquire a non-spherical shape during the solidification of the α-eicosene. Right: Droplets at $T \sim 30$ °C. Inset: Number distribution of the radius of the emulsion droplets from imaging particle analysis at $T \sim 30$ °C. The solid line shows a fit with a Schulz distributions $N(R)$ with an average radius of $\overline{R} = 1.68\,\mu m$ and a polydispersity of $\sigma = 0.195$ (standard deviation) with $N(R) = \frac{R^z}{z!}\left(\frac{z+1}{\overline{R}}\right)^{z+1} \exp\left[-\frac{R}{\overline{R}}(z+1)\right]$ and $z = 1/\sigma^2 - 1$.

several days up to weeks but observe signs of droplet coalescence after about 8 weeks. Emulsions were stored in an oven well above the melting point at around T≃40 °C at an approximate volume fraction of 40%. Drying was prevented by careful sealing. In order to induce a sharp and sufficiently fast transition, we take measurements at $T = 15$ °C, well below the bulk melting transition temperature to avoid the influence of possible droplet size effects on the melting temperature T_c and to make sure that the solid α-eicosene phase is rapidly reached. This way we can also exclude that the wax in some of the droplets could remain trapped in a supercooled liquid state for an extended period of time. By visual inspection we can readily observe that the droplets turn into solid wax particles. In microscopy we also observe that the solidification can induce a shape change of the particles, Fig. 1. We note that these shape changes were already reported in [23]. The formation of faceted and disc like shapes can be explained by the fact that the liquid to solid phase transition is most likely liquid to a smectic-like rotator phase of a liquid crystal [23]. These disc like particles are then optically anisotropic, exhibiting interesting light–dark birefringence while rotationally and translationally diffusing in cross-polarized light [23].

In general, this means that for $T = 30$ °C, above the transition temperature, the liquid α-eicosene droplets retain a nearly spherical shape while at the lower set-point $T = 15$ °C, the α-eicosene has turned into solid wax and the particle shape slowly evolves over many hours to days, becoming less spherical and even exhibiting facets. Moreover, the stabilization of the α-eicosene by the SDS surfactant layer at the liquid-liquid interface is likely not retained in the same way as in the liquid state of α-eicosene-in-water. Nonetheless, as we will show later in the text, both at $T = 15$ °C and $T = 30$ °C we find stable dispersions and the Brownian motion probed by dynamic multiple light scattering (DWS) shows no signature of aggregation or phase separation. Although the SDS concentration is slightly above the critical micelle concentration around 8 mM, any residual micelle-induced depletion attractions between droplets are weak compared to k_BT. In the following we study the properties of dispersions or emulsions for volume fractions ranging from $\phi = 0.1 \rightarrow 0.6$. The α-eicosene weight fraction of a concentrated stock emulsion is determined by drying and weighing a sufficient amount of sample and from this we can determine the droplet volume fraction from the known densities of α-eicosene and water.

2.2. Methods

To gain access to the internal dynamic properties of our dense emulsion systems we perform dynamic light scattering experiments. Due to the strong multiple scattering of visible light, the dynamics of the system cannot be assessed using traditional dynamic light scattering methods or video microscopy. Instead, we use diffusing wave spectroscopy (DWS) [20,21], a dynamic light scattering technique that takes advantage of the diffuse scattering of light in turbid media. The intensity–intensity correlation function is recorded with a commercial DWS instrument (DWS RheoLab, LSInstruments AG, Switzerland), Fig. 2. Given the large size of the droplets we predominantly probe self-motion and shape fluctuations [22,28–30] while the contribution of collective motion to the dynamic multiple light scattering signal can be neglected. We can then express the measured and normalized intensity–intensity correlation function $g_2(t)$ as follows [28,30,31]:

$$g_2(t) - 1 = \left[\frac{(L/l^*+4/3)\sqrt{k_0^2 \langle \Delta \vec{r}^2_{app}(t) \rangle}}{\sinh[(L/l^*+4/3)\sqrt{k_0^2 \langle \Delta \vec{r}^2_{app}(t) \rangle}]} \right]^2 \quad (1)$$

Here $k_0 = 2\pi n/\lambda$ denotes the wavenumber of light, λ is the laser wavelength, n the refractive index of the continuous phase, l^* is the optical transport mean free path, L the cuvette path length and $\langle \Delta \vec{r}^2_{app}(t) \rangle$ the apparent average particle mean square displacement (msd). The measured photon count rate is proportional to the total transmission coefficient for diffusely scattered light T_λ, which in turn is given by $T_\lambda \propto l^*/L$. In the experiment $\langle \Delta \vec{r}^2_{app}(t) \rangle$ is extracted directly from the correlation function using the instrument software. By calibration, using a sample with a known value of l^*, we also gain access to the so-called transport mean free path of light of the samples at the wavelength of the laser employed, λ = 687 nm [28].

3. Results and discussion

3.1. Thermal motion probed by DWS

We study the thermal motion of the particles center of mass and fluctuations of the liquid interfaces. Given the significant polydispersity, crystallization of the particles is suppressed and, moreover, we only consider data for $\phi \leq 0.6$ where the dispersion is liquid. We note that for concentrations larger than $\phi \sim 0.65$ we do indeed observe the onset of elasticity both in rheology experiments and for DWS [32,1]. A quantitative study of this regime turned out to be very challenging due to the history dependence of the sample preparation and cooling/heating cycles. This interesting regime is thus beyond the scope of the present work but shall be addressed in a future publication if the experimental problems can be overcome.

Now we focus our attention on the *apparent* mean square displacement (msd) of the dispersed particles as obtained from the DWS experiments. The corresponding data is shown in Fig. 3. We expect the apparent msd to show simple center of mass diffusion $\langle \Delta \vec{r}^2(t) \rangle = 6D(\phi)t$ at intermediate time-scales $t \sim$ ms, determined by the short time diffusion coefficient $D(\phi)$. To be able to identify the onset of this regime we plot $\langle \Delta \vec{r}^2(t) \rangle / 6t$ and thus in the diffusive regime $\langle \Delta \vec{r}^2(t) \rangle / 6t$ = constant. In Fig. 3 we show the results obtained for the two different temperatures studied. Indeed, for intermediate and longer times we observe diffusive motion. At short times however we observe strong deviations from the plateau value, with clear differences between the two temperatures. For the solid wax particles at $T = 15$ °C the

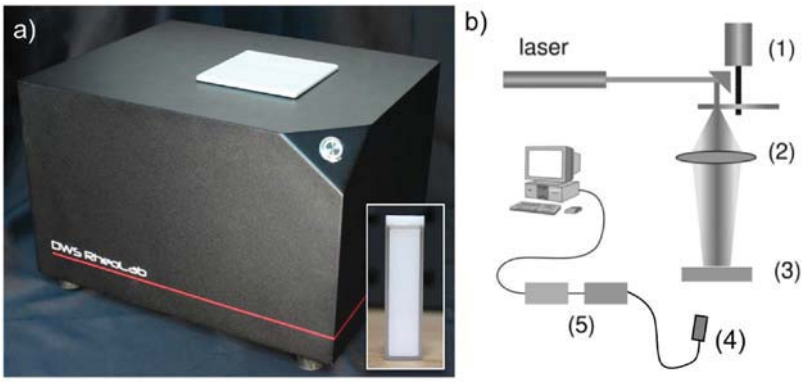

Fig. 2. Diffusing wave spectroscopy (DWS) setup. (a) Commercial DWS instrument (DWS RheoLab, LS Instruments, Switzerland). The inset shows a typical white sample contained in a $L = 5$ mm cuvette before loading the cuvette in the instrument [31]. (b) Optical configuration: A coherent light source (Laser, Cobolt, Sweden, λ = 687 nm) is directed to the surface of a ground glass diffuser mounted on a stepper motor (1). The speckle beam created by the diffuser is collimated by a lens (2) and then used to illuminate a sample cuvette containing the sample of interest (3). The sample holder is temperature controlled with $\Delta T < 0.1$ °C. The scattered light is collected by a single mode fiber receiver (4) in transmission and directed to a single photon counting module and digital correlator (5).

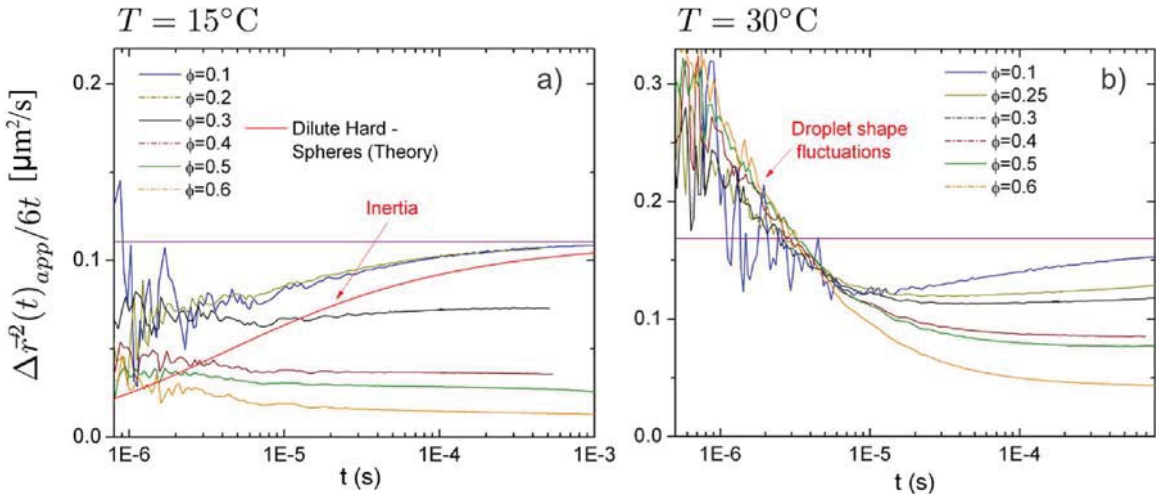

Fig. 3. Apparent mean square displacement of the droplets, mean radius $\overline{R} = 1.68\,\mu$m, obtained from the DWS measurements at different concentrations. The horizontal lines indicate the free diffusion coefficient $D_0 = k_B T/6\pi\eta\overline{R}$ in water at the given temperature, $D_0 \simeq 0.11\,\mu m^2/s$ for $T = 15\,^\circ$C and $D_0 \simeq 0.169\,\mu m^2/s$ for $T = 30\,^\circ$C. (a) Data taken at $T = 15\,^\circ$C. The solid red line shows the theoretical prediction by Hinch [33] for hard spheres taking account for the particle and fluid inertia. (b) Data taken at $T = 30\,^\circ$C.

curves tend toward zero for short times while for the liquid droplets we detect an upturn at short times. The former is a signature of droplet and fluid inertia [33] while the latter is characteristic for additional thermal fluctuations of the liquid droplet interface [22,29].

First we analyze the concentration dependence of the plateau values which should scale with the particle center of mass diffusion. We extract the plateau value $D(\phi)$ from the msd over the range $10^{-4} < t < 10^{-3}$ s. To be able to compare the two data sets in one graph, we plot $D(\phi)\eta(T)/T$ thereby taking into account the fact that the diffusion constant scales with the temperature and the viscosity η of the continuous phase: $D(\phi) \propto T/\eta(T)$. Indeed, as shown in Fig. 4, the high and the low temperature data collapse fairly well on a master curve. The collapse of the two data sets shows that the deformability of the interface has relatively little impact on the center-of-mass diffusion. As expected, the short time self-diffusion constant $D(\phi)$ decreases as the dispersion becomes more crowded. For a more quantitative analysis we compare the results to the semi-empirical expression by Lionberger and Russel [34]:

$$\frac{D(\phi)}{D_0} = \frac{1 - 1.56\phi}{1 - 0.27\phi} \tag{2}$$

The coefficient for unhindered free diffusion is given by the Stokes-Einstein relation $D_0 = K_B T/6\pi\eta\overline{R}$. We find good agreement with our experimental data if we assume a particle radius $\overline{R} \simeq 1.68\,\mu$m. The small differences between data and theory can be due to a number of reasons. The typical statistical error with respect to determining the l^* value of the sample is about 5–10%, Fig. 4b), and this uncertainty enters the analysis of $\langle \Delta\vec{r}^2_{app}(t) \rangle$ quadratically as can be seen from Eq. (1) [28,35]. The small differences can also be due to the fact that the DWS-weighted average size is slightly smaller than the number average $\overline{R}$ [36]. The experimental error in our $D(\phi)$ data, the size determination and influences due to polydispersity are all comparable. Therefore, a more complicated analysis, taking into account polydispersity, is beyond the scope of this work.

We now turn our attention to the behavior at very short times when approaching typical Brownian time scales, $t_B = m/6\pi\eta\overline{R} \sim 5{\cdot}10^{-7}S$, characterizing the relaxation of the particle velocity. Here m denotes the mass of the particle and $6\pi\eta R$ is the Stokes friction coefficient. While the msd-data at intermediate time scales are governed by the center of mass diffusion, we observe a dramatic change at short times where strong deviations from the plateau value can be noticed for $t < 10^{-5}$ s. Interestingly, for the solid wax particles and the liquid emulsion droplets, the data evolves in opposite directions. This can be understood in the following way. For hard, rigid, colloidal particles in low viscosity Newtonian solvents, such as water at ambient temperatures, contributions to the inertia of the particle and the displaced fluid

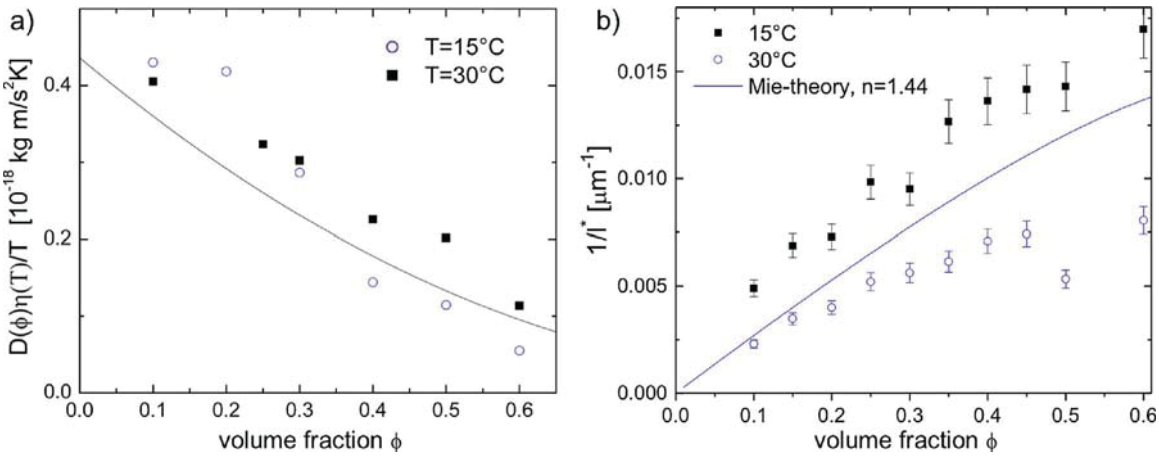

Fig. 4. (a) Scaled effective diffusion coefficient $D(\phi)\eta(T)/T$ extracted from the msd data shown in Fig. 3 for $T \sim 15\,^\circ$C and at $T \sim 30\,^\circ$C. Solid line: Lionberger Russel formula for hard spheres, Eq. (2). (b) Reciprocal optical transport mean free path of the emulsions at $T \sim 15\,^\circ$C and at $T \sim 30\,^\circ$C obtained from diffuse transmission measurements. The solid lines shows the prediction by Mie-theory at $\lambda = 687$ nm for monodisperse spherical droplets with a refractive index $n = 1.44$ dispersed in water $n = 1.332$.

lead to non-diffusive motion at short times. The principles of thermal Brownian motion can be understood in terms of a simple Langevin equation $m\partial^2\vec{r}\,(t)/\partial t^2 + 6\pi\eta R\partial\vec{r}\,(t)/\partial t = \vec{F_{\rm th}}(t)$ where m is the inertial mass of the particle, $\vec{F_{\rm fr}}\,(t) = 6\pi\eta R\partial\vec{r}\,(t)/\partial t$ is the Stokes friction force, and $\vec{F_{\rm th}}\,(t)$ is the force arising from random thermal fluctuations [37]. For a particle at long times $t\rightarrow\infty$ the motion is diffusive with $\langle\Delta\vec{r}^{\,2}(t)\rangle = 6Dt$. For extremely short times the motion becomes ballistic with $\langle\Delta\vec{r}^{\,2}(t)\rangle \propto t^2$. At intermediate times the time evolution depends on the details of the interaction between the particle and its surrounding fluid. In a simplified picture of Brownian motion the friction force acts instantaneously on a change of the particles velocity. However, when the particle receives momentum, it displaces the fluid in its immediate vicinity. The surrounding flow field is altered and acts back on the particle due to a non-negligible fluid inertia, as first described quantitatively by Hinch in 1975 [33,38]. The friction force then includes additional terms that depend on the particles past motion, which leads to a hydrodynamic memory effect and a corrected form of the Langevin approach [40]. Such a hydrodynamic effect delays the transition from ballistic to diffusive motion, resulting in a persistence of the nondiffusive motion to much longer times [38]. The full expression for an isolated particle, given by Hinch [33], is plotted in Fig. 3a) for the actual parameters of our wax particle dispersion ($\overline{R} = 1.68\,\mu$m).

At short times, shape fluctuations are a competing mechanism that can lead to thermally excited motion and they are a consequence of the deformability of the particles' interfaces and of the viscosity of the dispersed fluid. Fluctuations at an interface between a fluid and the solvent can be induced thermally as capillary waves. The amplitude of the wave is determined by deformability given by the surface tension of the droplet. The damping scales with the fluid viscosity. Interfacial motion can thus be thermally excited leading to shape fluctuations of the droplets on the nanoscale [22]. The standard DWS formalism does not consider shape fluctuations and here the additional motion simply show up as an apparent increase of displacement at short times. This additional contribution can be included as follows:

$$\langle\Delta\vec{r}^{\,2}_{\rm app}(t)\rangle = \langle\Delta\vec{r}^{\,2}(t)\rangle + \frac{3}{k_0^2(1-g)}\left[\frac{\Delta\sigma(0)-\Delta\sigma(t)}{\sigma_0}\right] = \langle\Delta\vec{r}^{\,2}(t)\rangle + f(t) \quad (3)$$

where $g = 1 - l_s/l^*$ denotes the scattering anisotropy parameter (i.e. the mean of the cosine of the scattering angle [39]) and l_s is the scattering mean free path. The magnitude and relaxation of the droplet shape fluctuations are described by the function $f(t) \propto (\Delta\sigma(0) - \Delta\sigma(t))/\sigma_0$. $\Delta\sigma(t)$ decays to zero and the entire function $f(t)$ plateaus after a characteristic relaxation time, in contrast to the center of mass displacement which is unbounded for a liquid emulsion. Therefore, the center of mass displacement dominates at long times. Whether the shape fluctuations are picked up by DWS or masked by the center of mass diffusion now depends on the magnitude of $f(t)$ and the relaxation time. A full theoretical analysis of the different contribution of the spectrum of excited modes to the shape fluctuations is reported in the work of Gang and coworkers [22]. For simplicity we only consider the principal relaxation mode $\Delta\sigma(t)/\Delta\sigma(0) = \exp(-t/\tau_{\rm sf})$ with a relaxation time of the dominant mode τ_{sf}. We can then express the contribution of the shape fluctuations to the apparent msd as

$$f(t) = \frac{3}{k_0^2(1-g)}\left[\frac{\Delta\sigma(0)-\Delta\sigma(t)}{\sigma_0}\right] \simeq A[1-\exp[-t/\tau_{\rm sf}]] \quad (4)$$

In the dilute limit, the amplitude of the fluctuations $A = 3\Delta\sigma(0)/\sigma_0 k_0^2(1-g)$ is predicted to scale inversely with the surface tension Γ and the relaxation time $\tau_{\rm sf}$ is proportional to the viscosity of the dispersed phase $\eta_{\rm wax}$ in the limit $\eta_{\rm WAX} > > \eta$. As shown in Fig. 5 our data for $\phi \geq 0.2$ is well described by Eqs. (3) and (4), assuming $\langle\Delta\vec{r}^{\,2}(t)\rangle/6t \sim$ const. This simplification is justified for the more concentrated emulsions $\phi \geq 0.2$ as can be seen in Fig. 3a) for the case of

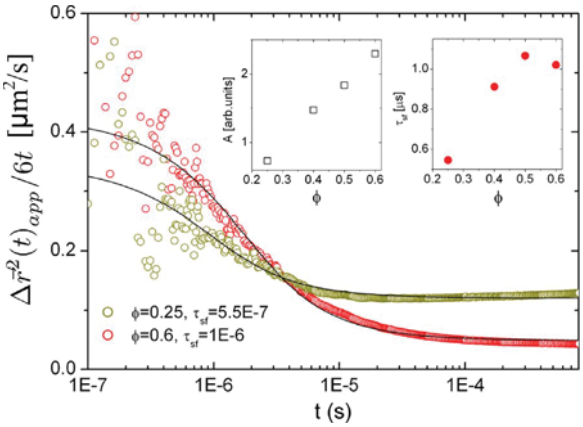

Fig. 5. Analysis of the contribution of shape fluctuations to the apparent mean square displacement of the droplets at $T \sim 30\,^{\circ}$C. Solid lines are fits to the data with Eq. (3), assuming $\langle\Delta\vec{r}^{\,2}(t)\rangle/6t \sim$ const. Inset: fit parameters A and τ_{sf} for different droplet volume fractions.

solid wax particles, i.e. in the absence of shape fluctuations. The relaxation times are found to be of the order μs, and the concentration dependence of $\tau_{\rm sf}$ and A shows a noticeable increase with ϕ, observations that all compare well to the results reported previously for simple emulsions that do not show solidification of the droplets for accessible temperatures, i.e. above the freezing point of the continuous phase $T > 0\,^{\circ}$C [22].

3.2. Scattering strength: transport mean free path

Finally, we analyze the results obtained for the reciprocal optical transport mean free path, Fig. 4b), which is a measure of the light scattering strength or optical density. The latter is a function of the volume fraction ϕ and droplet-droplet positional correlations [41]. For the roughly spherical objects studied here we can attempt to model l^* based on Mie scattering theory taking into account positional correlations via the well known Percus–Yevick structure factor $S(q)$ [42]. The latter has been shown previously to be a good model to describe the scattering from liquid emulsions below the jamming point $\phi < 0.6$ [43]. Here we find that both the high and the low temperature data are fairly well described by such a model based on a single mean droplet size $\overline{R} = 1.68\,\mu$m and using the tabulated refractive index of the $\alpha-$eicosene $n = 1.44$ for visible light [24] dispersed in water $n = 1.33$. We have also checked that the finite polydispersity does not alter the predicted results (based on Mie-theory) by more than 10% and thus, for simplicity, we have neglected its influence [36].

Positional correlations and loss of contrast lead to a deviation of the linear scaling of the optical density $1/l^* \propto \phi$. As we can see from Fig. 4b), such deviations are moderate and both data sets show a steady, nearly linear, increase up to concentrations on the order of $\phi = 0.5$. This is typically observed for particles with a size significantly larger than the wavelength of light $R > > \lambda$ [44]. Interestingly the slope of $1/l^* \propto \phi$ is slightly higher for the solid wax particles at the lower temperature of $T = 15\,^{\circ}$C. This indicates that the individual particle scattering properties change after the $\alpha-$eicosene has solidified. A possible reason for this change would be a slightly increased particle refractive index when the wax solidifies or fluctuations of the optical axis in a smectic liquid crystalline phase [23]. Based on the measurements of the Brownian diffusion coefficient, shown in Fig. 4a), it appears unlikely that a significant size change of the wax particles is responsible for the enhanced scattering.

4. Summary and conclusions

In conclusion we have shown that a uniform microscale emulsion of

α-eicosene wax droplets dispersed in an aqueous SDS solution is an interesting colloidal model system with tunable properties of constituent droplets from deformable to rigid. Over a wide range of droplet volume fractions below jamming, the droplets either mimic the behavior of solid spheres for temperatures below T_c, or the behavior of liquid droplets for temperatures above T_c. We have shown that DWS can capture the microscopic dynamics at the microsecond scale and we could identify the contribution of center of mass diffusion and shape fluctuations of the liquid droplets over the whole range, consistent with prior studies on non-waxy emulsions. Yet, when we lower the temperature below T_c, these shape fluctuations freeze out, and the thermal motion can be attributed to the center of mass displacement alone. This transition is fully reversible and therefore particle softness, that manifests itself via shape fluctuations of the droplets, can be dialed in and out at will. Thus, this system or others like it could potentially provide an interesting playground for testing models and concepts of the glass and the jamming transition in even denser suspensions, for $\phi > \phi_{rcp} \sim 0.64$, that critically rely on the softness of constituent particles. However, the solidification of the eicosene wax and the subsequent shape changes may complicate the use of this material for such purposes. Thus, the reversibility of the transition is limited only over certain time scales after the temperature change, since the droplets can evolve into faceted or disc-like shapes. Moreover, in tandem with the faceting of the particles, solidification driven shape-changes of particles may alter particle–particle interactions, potentially leading to a weakly attractive component that may depend on the shapes and orientations of interacting wax particles. We anticipate that measuring and interpreting early-time DWS msds could potentially yield quantitative information about the high frequency viscoelasticity of the internal contents of dispersed colloidal objects of other types of soft materials, beyond simple hydrocarbon waxes.

Acknowledgements

FS, CL, ZC acknowledge financial support from the Swiss National Science Foundation via Project Nos. 149867, 142571 and 169074. This project has also benefitted from support from the Swiss National Science Foundation via the National Center of Competence in Research Bio-Inspired Materials. JY acknowledges financial support by the University of Fribourg and the Fribourg Center for Nanomaterials (FriMat). KH Ahn acknowledges the support from the National Research Foundation of Korea (NRF) funded by the Korea government (MSIP) (No. 2016R1E1A1A01942362).

References

[1] T.G. Mason, J. Bibette, D.A. Weitz, Elasticity of compressed emulsions, Phys. Rev. Lett. 75 (10) (1995) 2051.
[2] D. Schuster, Encyclopedia of Emulsion Technology vol. 4, CRC Press, 1996.
[3] G.M. Conley, P. Aebischer, S. Nöjd, P. Schurtenberger, F. Scheffold, Jamming and overpacking fuzzy microgels: deformation, interpenetration, and compression, Sci. Adv. 3 (10) (2017) e1700969.
[4] P.S. Mohanty, S. Nöjd, K. van Gruijthuijsen, J.J. Crassous, M. Obiols-Rabasa, R. Schweins, A. Stradner, P. Schurtenberger, Interpenetration of polymeric microgels at ultrahigh densities, Sci. Rep. 7 (2017) 1487.
[5] N. Koumakis, A. Pamvouxoglou, A. Poulos, G. Petekidis, Direct comparison of the rheology of model hard and soft particle glasses, Soft Matter 8 (15) (2012) 4271–4284.
[6] C. Pellet, M. Cloitre, The glass and jamming transitions of soft polyelectrolyte microgel suspensions, Soft Matter 12 (16) (2016) 3710–3720.
[7] A. Fernandez-Nieves, H. Wyss, J. Mattsson, D.A. Weitz, Microgel Suspensions: Fundamentals and Applications, John Wiley & Sons, 2011.
[8] R. Hidalgo-Álvarez, Structure and Functional Properties of Colloidal Systems vol. 146, CRC Press, 2009.
[9] M. Braibanti, H.S. Kim, N. Şenbil, M.J. Pagenkopp, T.G. Mason, F. Scheffold, The liquid–glass–jamming transition in disordered ionic nanoemulsions, Sci. Rep. 7 (1) (2017) 13879.
[10] P.N. Pusey, W. van Megen, Phase behaviour of concentrated suspensions of nearly hard colloidal spheres, Nature 320 (6060) (1986) 340–342.
[11] G. Brambilla, D. El Masri, M. Pierno, L. Berthier, L. Cipelletti, G. Petekidis, A.B. Schofield, Probing the equilibrium dynamics of colloidal hard spheres above the mode-coupling glass transition, Phys. Rev. Lett. 102 (8) (2009) 085703.
[12] K. Pham, G. Petekidis, D. Vlassopoulos, S. Egelhaaf, P. Pusey, W. Poon, Yielding of colloidal glasses, EPL (Europhys. Lett.) 75 (4) (2006) 624.
[13] A.P. Gast, W.B. Russel, Simple ordering in complex fluids, Phys. Today 51 (1998) 24–31.
[14] P. Bartlett, R. Ottewill, P. Pusey, Freezing of binary mixtures of colloidal hard spheres, J. Chem. Phys. 93 (2) (1990) 1299–1312.
[15] W.C. Poon, E.R. Weeks, C.P. Royall, On measuring colloidal volume fractions, Soft Matter 8 (1) (2012) 21–30.
[16] J.R. Seth, L. Mohan, C. Locatelli-Champagne, M. Cloitre, R.T. Bonnecaze, A micromechanical model to predict the flow of soft particle glasses, Nat. Mater. 10 (11) (2011) 838–843.
[17] A. Ikeda, L. Berthier, P. Sollich, Disentangling glass and jamming physics in the rheology of soft materials, Soft Matter 9 (32) (2013) 7669–7683.
[18] A.J. Liu, S.R. Nagel, The jamming transition and the marginally jammed solid, Annu. Rev. Condens. Matter Phys. 1 (1) (2010) 347–369.
[19] P. Olsson, S. Teitel, Critical scaling of shear viscosity at the jamming transition, Phys. Rev. Lett. 99 (17) (2007) 178001.
[20] G. Maret, P. Wolf, Multiple light scattering from disordered media. the effect of Brownian motion of scatterers, Z. Phys. B: Condens. Matter 65 (4) (1987) 409–413.
[21] D. Pine, D.A. Weitz, P. Chaikin, E. Herbolzheimer, Diffusing wave spectroscopy, Phys. Rev. Lett. 60 (12) (1988) 1134.
[22] H. Gang, A. Krall, D.A. Weitz, Shape fluctuations of interacting fluid droplets, Phys. Rev. Lett. 73 (25) (1994) 3435.
[23] T.G. Mason, Osmotically driven shape-dependent colloidal separations, Phys. Rev. E 66 (6) (2002) 060402.
[24] W.M. Haynes, CRC Handbook of Chemistry and Physics, CRC Press, 2014.
[25] F. Scheffold, J.N. Wilking, J. Haberko, F. Cardinaux, T.G. Mason, The jamming elasticity of emulsions stabilized by ionic surfactants, Soft Matter 10 (28) (2014) 5040–5044.
[26] J. Bibette, Depletion interactions and fractionated crystallization for polydisperse emulsion purification, J. Colloid Interface Sci. 147 (2) (1991) 474–478.
[27] A.F. Mejia, P. He, D. Luo, M. Marquez, Z. Cheng, Uniform discotic wax particles via electrospray emulsification, J. Colloid Interface Sci. 334 (1) (2009) 22–28.
[28] F. Scheffold, P. Schurtenberger, Light scattering probes of viscoelastic fluids and solids, Soft Mater. 1 (2) (2003) 139–165.
[29] H. Gang, A. Krall, D.A. Weitz, Thermal fluctuations of the shapes of droplets in dense and compressed emulsions, Phys. Rev. E 52 (6) (1995) 6289.
[30] W. Brown, Dynamic Light Scattering: The Method and Some Applications vol. 49, Oxford University Press, USA, 1993.
[31] C. Zhang, M. Reufer, D. Gaudino, F. Scheffold, Improved diffusing wave spectroscopy based on the automatized determination of the optical transport and absorption mean free path, Korea-Aust. Rheol. J. 29 (4) (2017) 241–247.
[32] F. Scheffold, F. Cardinaux, T.G. Mason, Linear and nonlinear rheology of dense emulsions across the glass and the jamming regimes, J. Phys.: Condens. Matter 25 (50) (2013) 502101.
[33] E. Hinch, Application of the Langevin equation to fluid suspensions, J. Fluid Mech. 72 (03) (1975) 499–511.
[34] A.J. Banchio, G. Nägele, Short-time transport properties in dense suspensions: from neutral to charge-stabilized colloidal spheres, J. Chem. Phys. 128 (10) (2008) 104903.
[35] P. Kaplan, M.H. Kao, A. Yodh, D.J. Pine, Geometric constraints for the design of diffusing-wave spectroscopy experiments, Appl. Opt. 32 (21) (1993) 3828–3836.
[36] F. Scheffold, Particle sizing with diffusing wave spectroscopy, J. Dispers. Sci. Technol. 23 (5) (2002) 591–599.
[37] R. Zwanzig, Nonequilibrium Statistical Mechanics, Oxford University Press, 2001.
[38] D.A. Weitz, D. Pine, P. Pusey, R. Tough, Nondiffusive Brownian motion studied by diffusing-wave spectroscopy, Phys. Rev. Lett. 63 (16) (1989) 1747.
[39] L.F. Rojas-Ochoa, D. Lacoste, R. Lenke, P. Schurtenberger, F. Scheffold, Depolarization of backscattered linearly polarized light, J. Opt. Soc. Am. A 21 (9) (2004) 1799–1804.
[40] R. Huang, I. Chavez, K.M. Taute, B. Lukić, S. Jeney, M.G. Raizen, E.-L. Florin, Direct observation of the full transition from ballistic to diffusive Brownian motion in a liquid, Nat. Phys. 7 (7) (2011) 576–580.
[41] L. Rojas-Ochoa, S. Romer, F. Scheffold, P. Schurtenberger, Diffusing wave spectroscopy and small-angle neutron scattering from concentrated colloidal suspensions, Phys. Rev. E 65 (5) (2002) 051403.
[42] J.-P. Hansen, I.R. McDonald, Theory of Simple Liquids, Elsevier, 1990.
[43] F. Scheffold, T.G. Mason, Scattering from highly packed disordered colloids, J. Phys.: Condens. Matter 21 (33) (2009) 332102.
[44] S. Fraden, G. Maret, Multiple light scattering from concentrated, interacting suspensions, Phys. Rev. Lett. 65 (4) (1990) 512.